World Academy of Science, Engineering and Technology
International Journal of Mechanical and Mechatronics Engineering
Vol:3, No:5, 2009

Improvement of Passengers Ride Comfort in Rail Vehicles Equipped with Air Springs

H. Sayyaadi, and N. Shokouhi

***Abstract*—**In rail vehicles, air springs are very important isolating component, which guarantee good ride comfort for passengers during their trip. In the most new rail–vehicle models, developed by researchers, the thermo–dynamical effects of air springs are ignored and secondary suspension is modeled by simple springs and dampers. As the performance of suspension components have significant effects on rail–vehicle dynamics and ride comfort of passengers, a complete nonlinear thermo–dynamical air spring model, which is a combination of two different models, is introduced. Result from field test shows remarkable agreement between proposed model and experimental data. Effects of air suspension parameters on the system performances are investigated here and then these parameters are tuned to minimize Sperling ride comfort index during the trip. Results showed that by modification of air suspension parameters, passengers comfort is improved and ride comfort index is reduced about 10%.

***Keywords*—**Air spring, Ride comfort improvement, Thermo–dynamical effects.

I. Introduction

NOWADAYS, speed up in technology and its new features bring higher speed, with reliable safety and better ride comfort in rail transportation industries. Traffic jam in capital cities all around the world, wasting passengers' time at the airports, huge mass transportation and so on bring a good opportunity for rail industries to attract more and more passengers and cargos to their services. In addition to safety, the other important issue for passengers to decide about transportation type is ride comfort during their trip. And that is why accessing better ride comfort during the trip for passengers is essential.

To serve good ride comfort to the passengers, the secondary suspension of most new EMU and DMU rail–vehicles is equipped with air springs. Air springs are very important isolation component, which guarantee good ride comfort during the trip.

Air springs, which are made of Carbon Black Filled Natural Rubber (CBNFR), have long lifetime and isolate the vehicle body from the unpredictable noise and vibration. The air springs' behaviors are so complicated that cannot be modeled by simple equations. In the most new rail–vehicle models, developed by researchers [1]-[7], the thermo–dynamical effects of air springs are ignored and secondary suspension is modeled by simple springs and dampers. The air spring response is independent of the excitation frequency [8] and it behaves such as stress relaxation function [9]. In addition, it has asymmetric hysteresis loop, which is independent of the excitation frequency [10]. These behaviors bring difficulties for using frictional or columbic description to approximate the air spring characteristics. Stress relaxation function of CBNFR rubbers is shown in Fig. 1.

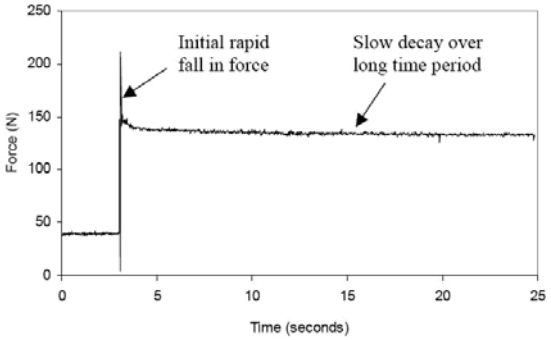

Fig. 1 Stress relaxation response [9]

CBFNR response to cyclic excitation has asymmetric hysteresis loops, which is independent of excitation frequency. This characteristic has been reported many times by different researchers [10], [12]. Fig. 2 shows the typical asymmetric hysteresis loop of CBFNR rubbers.

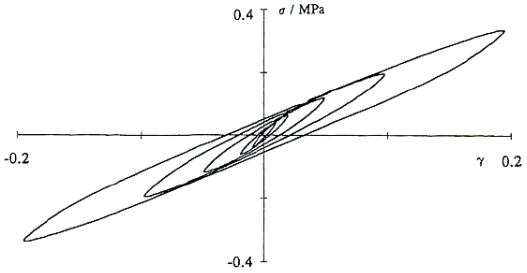

Fig. 2 CBFNR hysteresis loops [11]

II. Air Spring Models

For modeling CBFNR behavior, a model is introduced by Turner [11] and further developed by Coveney and Johnson [12]. In that model named Triboelastic, a large number of microscopic, one dimensional, coulombic elements, linked by

H. Sayyaadi is associate professor in Mechanical Engineering Department, Sharif University of Technology, Azadi Avenue, P.O.Box: 11365-9567, Tehran, Iran (phone:+98-21-66165682, fax:+98-21-66000021, e-mail Address: sayyaadi@sharif.edu

N. Shokouhi is Ph.D. student in Mechanical Engineering Department, Sharif University of Technology, Tehran, Iran, and cooperates with Irankhodro Rail Transport Industries Co. (IRICo), (e-mail address: n_shokouhi@mech.sharif.edu).

springs, are implemented which the resulting friction force is proportional to square root of current and previous turning point displacement differences.

Coveney and Johnson [13] modified the Triboelastic model and developed two new models named Triboelastic visco–solid (TVS) and Rate dependent Triboelastic (RT) models. The TVS is the same as berg model [10], while in the RT model; the Triboelastic element is replaced with a non–linear Maxwell element. TVS model has not asymmetric hysteresis loop, which causes rapid change in force vector. Also, the model parameters cannot easily be adjusted.

Bergstrom and Boyce [14], developed a different model similar to Triboelastic RT model with two differences; equilibrium response is described by a hyper–elastic model and time dependent response is a function of both velocity and displacement raised to a power. This model still has some difficulties to implement in dynamic analysis.

Miehe and Keck [15] introduced a model, which is similar to the Berg and TVS model. This model has 20 parameters, which made it very difficult to define these all parameters value.

Lion [16] proposed a phenomenological model with non–linear elasticity, non–linear plastic hysteresis, non–linear visco–elasticity and stress softening which has modular components, the same as Miehe and Keck model, but different in functions. The equations given for this model are very difficult to be implemented in the dynamic analysis.

In the latest 3D model, developed by Berg [17], the effects of elasticity, friction and viscosity of air spring in vertical, lateral and longitudinal directions are introduced. In that model, the stress relaxation response is not represented. The complete explanation about this model, shown in Fig. 3, can be found in [17]. Friction force in this model is defined by the following function, which is zero at turning points.

$$F_{Friction} \propto \frac{(x-x_0)}{\beta+(x-x_0)}.sign(\dot{x}) \qquad (1)$$

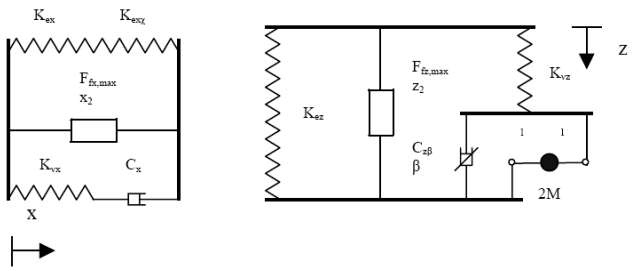

Fig. 3 Berg model [17]

In the above equation, β is constant, x is current displacement and x_0 is the displacement at the previous turning point. It is clear that in this model, displacement at turning points should be detected and assigned to the x_0 variable, which is not a standard procedure in the dynamic analysis and causes failure in solving algorithm.

For simulation of CBFNR rubber behavior, a model was developed by Haupt & Sedlan [9] which has elastic and viscoelastic elements. The viscoelastic element naturally produces asymmetric stress–strain response and is weakly time–dependent. These features are not presented in the other models and made it very powerful to simulate the CBFNR behaviors. Simplified one–dimensional Haupt & Sedlan model with constant coefficients is shown in Fig. 4.

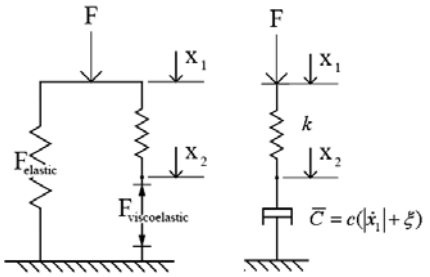

Fig. 4 One–dimensional Haupt & Sedlan model

The simplified viscoelastic force in this model is described by the following function:

$$F_{visco-elastic} = \frac{c\,\dot{x}_2}{|\dot{x}_1|+\zeta} \qquad (2)$$

Where c and ζ are constant. Equation (2) is simply a standard linear Maxwell element where the viscous force is divided to the magnitude of strain rate and a constant.

In this research work, Berg model which is validated by some experimental data up to 16 Hz frequencies [17], is used to simulate the air spring behaviors. However, because of difficulties comprises from assigning previous turning point displacement to the variable, the frictional part of this model is replaced by the simplified viscoelastic model defined by Haupt & Sedlan. Schematic diagrams of modified models in vertical and lateral directions are shown in Fig. 5.

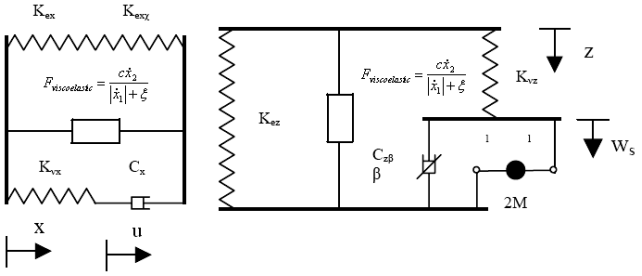

Fig. 5 Proposed modified model for air spring

According to Berg and by taking into consideration of Haupt & Sedlan model, differential equations of air spring behavior in vertical, lateral and longitudinal directions are determined as follows:

Vertical direction:

$$M\,\ddot{w}_s = K_{vz}(z-w_s) - C_{z\beta}|\dot{w}_s|^{\beta} sign(\dot{w}_s), \qquad \beta = 1.8 \qquad (3)$$

$$F_z = (p_0 - p_a)A_e + K_{ez}z + K_{vz}(z-w_s) + \frac{c\,\dot{x}_2}{|\dot{z}|+\zeta} \qquad (4)$$

Lateral and longitudinal directions:

$$F_w = K_{ew}w + K_{ew\chi}\theta + F_{visco-elastic,w} + K_{vw}(w-u) \qquad (5)$$

$$C_w\dot{u} = K_{vw}(w-u) \qquad (6)$$

And

$$F_{visco-elastic,w} = \frac{c\,\dot{x}_2}{|\dot{w}_1| + \zeta}, \quad w = x,\ y \tag{7}$$

Numerical values of the above parameters are estimated by the following equations [18]:

$$M = l_s A_s \rho \left(\frac{A_e}{A_s} \frac{V_{r0}}{V_{b0} + V_{r0}} \right)^2 \tag{8}$$

$$K_{ez} = \left(\frac{1}{\frac{p_0 A_e^2 n}{V_{b0} + V_{r0}} + p_g \frac{dA_e}{dz}} + \frac{1}{K_{auxiliary}} \right)^{-1} \tag{9}$$

$$K_{vz} = \left(\frac{1}{\frac{p_0 A_e^2 n}{V_{b0}} + p_g \frac{dA_e}{dz}} + \frac{1}{K_{auxiliary}} \right)^{-1} - K_{ez} \tag{10}$$

$$C_{z,\beta} = \frac{1}{2} \rho . k_t . A_s \left(\frac{A_e}{A_s} \frac{V_{r0}}{V_{b0} + V_{r0}} \right)^{1+\beta}, \ \beta = 2 \tag{11}$$

The exact $C_{z,1.8}$ value is calculated according to the Presthus method and the stiffness $K_{ex\chi}$ can be approximated by $K_{ex\chi} = 0.7(K_{ex} h + load)$ [18]. The parameters of IRICo DMU air springs in the above equations are described in Table I.

TABLE I
AIR SPRING PARAMETERS VALUE

Parameters	Description	Values
l_s	Connecting pipe length	3.2 m
A_s	Connecting pipe cross section	0.001359 m^2
A_e	Effective area of the air spring	0.291 m^2
P_0	Initial absolute pressure	3.806 bar
P_q	Gauge pressure	–
ρ	Density of the air at P_0 pressure	4.523 kg/m^3
V_{r0}	Reservoir volume	0.040 m^2
V_{b0}	Air spring volume	0.064 m^2
k_t	Total lost coefficient	3.4727
$K_{auxiliary}$	Auxiliary spring stiffness	8234 kN/m
M	Air mass	198.385 kg

III. Model Simulation and Validations

To simulate dynamic behavior of air spring, a model is developed in Matlab/Simulink software. For evaluating performance of the developed model, bogie side states are fixed to constant and response of air spring to sinusoidal movement of carbody side states in vertical and lateral directions are investigated.

To determine the exact values of the air spring parameters, real test of IRICo DMU air spring is carried out at ContiTech Company, Germany. The test carried out with amplitude of ±10 mm between 0.5 and 10 Hz frequencies. Fig. 6 depicts the air spring test.

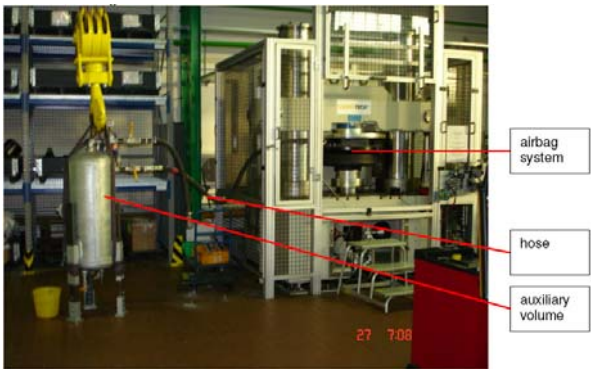

Fig. 6 Test rig of air spring at ContiTech Company, Germany

Based on the method introduced by Docquier [19], vertical dynamic stiffness of air spring and loss angle, as are shown in Fig. 7 and Fig. 8, are investigated.

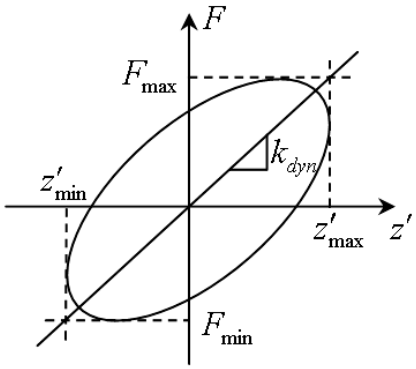

$$k_{dyn} = \frac{F_{\max} - F_{\min}}{z'_{\max} - z'_{\min}}$$

Fig. 7 Dynamic vertical stiffness of air spring [19]

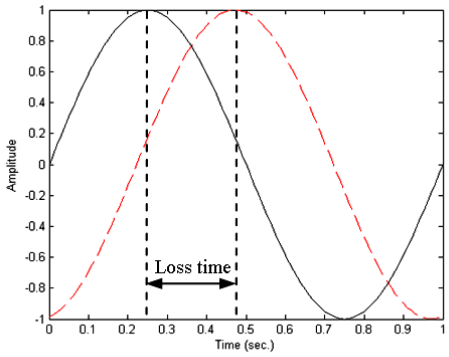

$$D_{Loss\ Angle} = 2\pi f T_{Loss\ time}$$

Fig. 8 Loss angle

According to the real test data and simulation results, loss angle and vertical dynamic stiffness of air spring are calculated which are shown in Fig. 9 and Fig. 10. As it can be seen, good agreement between real test and simulation results is achieved.

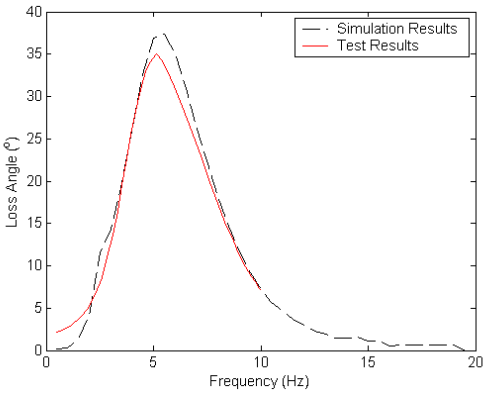

Fig. 9 Loss angle of air spring - $M = 198.385\ kg$, $K_{ez} = 461.629\ N/mm$, $K_{vz} = 351.185\ N/mm$, $C_{z,1.8} = 11.508\ kN(s/m)^{1.8}$ $k_{haupt} = 96\ kN/m$, $C_{haupt} = 1.52\ kNs/m$, $\zeta = 0.00063$

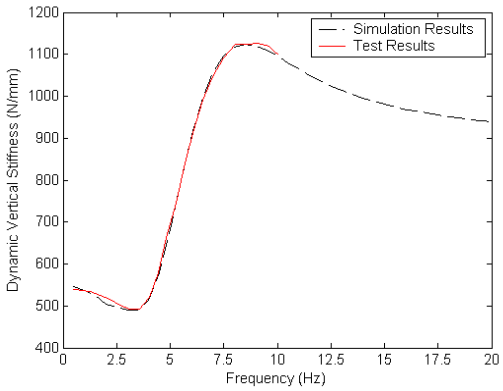

Fig. 10 Dynamic vertical stiffness $M = 198.385\ kg$, $K_{ez} = 461.629\ N/mm$, $K_{vz} = 351.185\ N/mm$, $C_{z,1.8} = 11.508\ kN(s/m)^{1.8}$, $k_{haupt} = 96\ kN/m$, $C_{haupt} = 1.52\ kNs/m$, $\zeta = 0.00063$

For validation of lateral behavior, hysteresis loop of air spring is evaluated. Results are shown in Fig. 11.

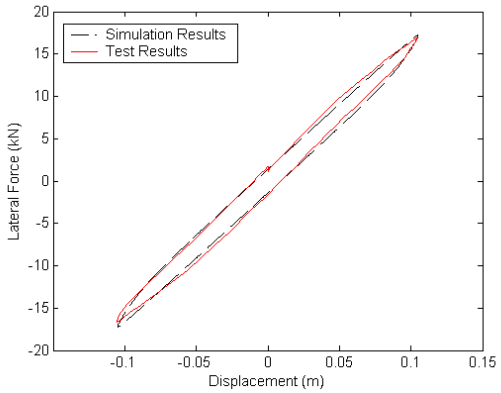

Fig. 11 Hysteresis loop of the air spring in lateral direction, $K_{ey} = 154\ kN/m$, $K_{vy} = 82.26\ kN/m$, $C_y = 1.109\ kNs/m$, $k_{haupt} = 96\ kN/m$, $C_{haupt} = 1.52\ kNs/m$, $\zeta = 0.00063$

Good agreement between real test data and simulation results shows that proposed equations can simulate the real behavior of air spring very well.

IV. Air Reservoir Volume and Connecting Pipes' Influences

In this section, the influence of rail–vehicle secondary suspension parameters on the performance of air spring, including air reservoir volume and connecting pipes' length and diameter, will be discussed.

A. Air Reservoir Volume

Performance of air springs is highly affected by air reservoir volume. For studding the influences of air reservoir volume on the system performances, dynamic stiffness and loss angle of air spring reaction force for various air reservoir volumes are studied within 0~20 Hz excitation frequencies as shown in Fig. 12 and Fig. 13. As it can be seen, by adjusting air reservoir volume to zero, the air spring behaves as a simple stiffness component and loss angle of reaction force is zero for all excitation frequencies. This indicates that no damping characteristic is exists in the system when air reservoir volume is zero.

By increasing air reservoir volume, dynamic stiffness graph is divided to low, transient and high frequency sections and damping characteristic is appended to the system in shape of loss angle within specific frequency range. At the same time, For higher air reservoir volume, maximum loss angle is occurred at lower frequencies with higher amplitude, as increasing air reservoir volume from 5 to 80 liters, increases maximum loss angle from 15.7° at 14.5 Hz to 48.1° at 4 Hz frequency.

Furthermore, when air reservoir volume is increased, dynamic stiffness of system is decreased at low frequencies and increased at high frequencies. So, by identifying resonance frequency of rail–vehicle, transient section of air spring response can be adjusted so that vehicle responses be restricted.

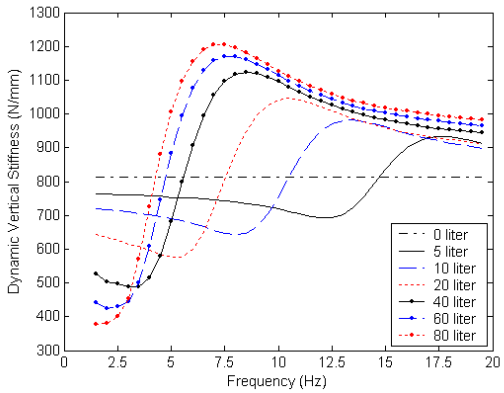

Fig. 12 Dynamic vertical Stiffness of air spring for various air reservoir volumes

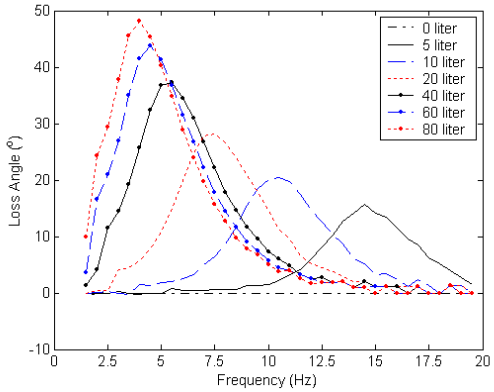

Fig. 13 Loss angle of air spring for various air reservoir volumes

B. Connecting Pipe Diameter

As it can be seen in Fig. 14, by increasing connecting pipe diameter, the transient section of air spring dynamic stiffness is shifted to higher frequencies. The same concept is valid for loss angle as shown in Fig. 15. By increasing connecting pipe diameter, maximum loss angle is shifted to higher frequencies with higher amplitude.

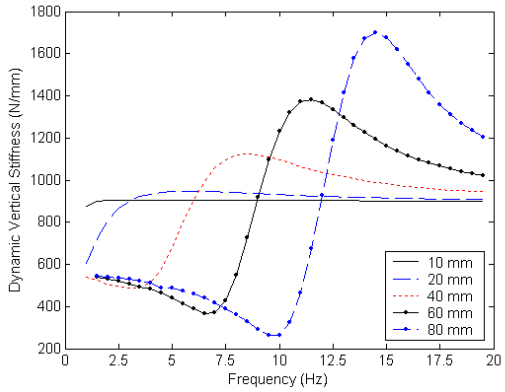

Fig. 14 Dynamic vertical Stiffness of air spring for various pipe diameters

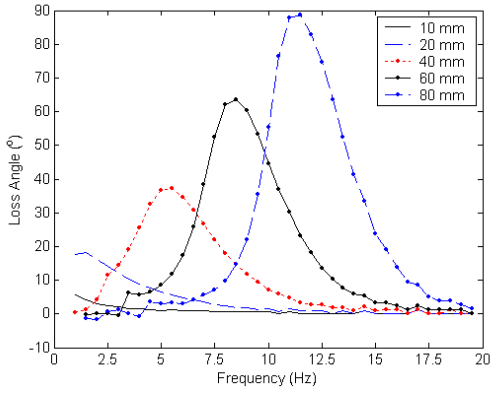

Fig. 15 Loss angle of air spring for various pipe diameters

Whereas increasing air reservoir volume shifts the graphs to the lower frequencies, increasing connecting pipe diameter shifts the graphs to the higher frequencies. Comparison of reservoir volume and connecting pipe diameter influences shows that both factors add a damping characteristic to the system.

C. Connecting Pipes' Length

Dynamic stiffness and loss angle of air spring for different connecting pipes' lengths are shown in Fig. 16 and Fig. 17. By increasing connecting pipes' length, dynamic stiffness and loss angle graphs are widened. As it can be seen, for all connecting pipes' lengths, low frequency section almost remained unchanged. Furthermore, transient section is widened and high frequency section is shifted to higher frequencies. So by adjusting connecting pipes' length, damping characteristic of air spring can cover wider range of excitation frequencies.

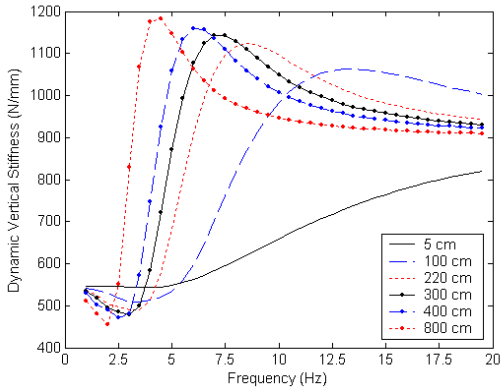

Fig. 16 Dynamic vertical Stiffness of air spring for various pipe lengths

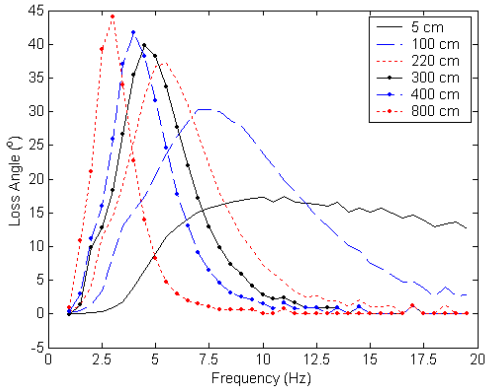

Fig. 17 Loss angle of air spring for various pipe lengths

V. Vehicle Model

For evaluating air suspension performances, one IRICo DMU rail vehicle is modeled. IRICo DMU is composed of four cars; two motor cars at each end and two trailer cars in the middle. The composition of one complete train is shown in Fig. 18. Complete explanation about developed model and its validation can be found in [20].

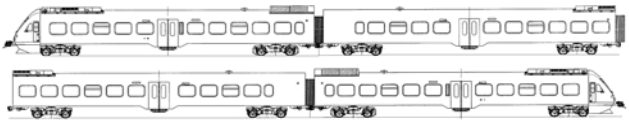

Fig. 18 Composition of IRICo DMU

VI. Passengers' Comfort Improvement

In this section, air suspension parameters of rail vehicles are tuned so that good ride comfort for passengers is guaranteed during their trip. Accordingly, performances of air suspension system in rail vehicles are investigated. Power Spectral Density (PSD) of first axle, front bogie frame and carbody vertical accelerations for real air suspension parameters are shown in Fig. 19. As it can be seen from this figure, carbody is excited strongly between 1.5 and 3 Hz frequencies.

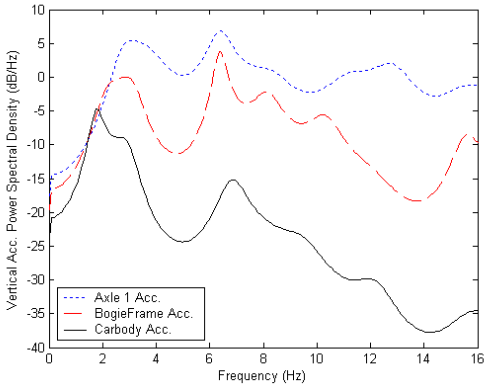

Fig. 19 PSD diagram of first axle, front bogie frame and carbody vertical accelerations (with 80 km/h speed)

For real air suspension parameters, maximum loss angle appears around 6 Hz frequencies as shown in Fig. 20.

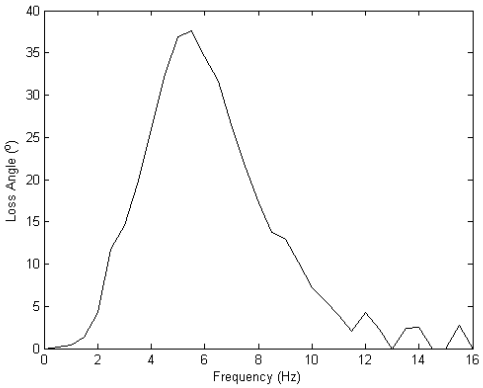

Fig. 20 Loss Angle of air spring response
$V_{normal} = 40\,Lit,\ L_{normal} = 2200\ mm, D_{normal} = 40\,mm$

Whereas secondary air suspension, damps vertical excitations around 6 Hz frequencies, carbody vertical acceleration has no significant excitation within this range. So, capabilities of air suspension system for damping carbody vertical vibrations in the modeled rail vehicle are not well employed. Carbody is exited with maximum amplitude within 1.5 and 3 Hz frequencies, as shown in Fig. 19, which should be damped with secondary air suspension system.

To reduce transmitted vertical vibrations to the carbody, air suspension parameters of the modeled rail vehicle are tuned so that maximum loss angle occurs at lower frequencies as shown in Fig. 21.

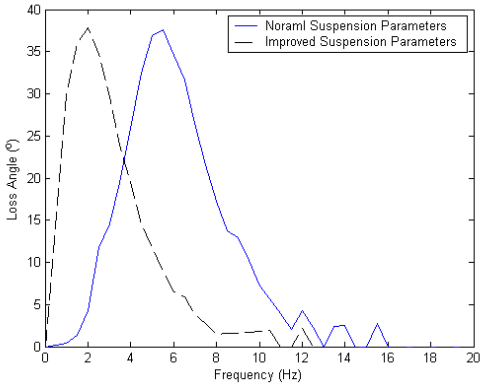

Fig. 21 Loss Angle of air spring response
$V_{normal} = 40\,Lit,\ L_{normal} = 2200\ mm, D_{normal} = 40\,mm$
$V_{improved} = 100\,Lit,\ L_{improved} = 3200\ mm, D_{improved} = 30\,mm$

As it can be seen, by increasing air reservoir volume from 40 lit to 100 liter, increasing connection pipe length from 2.2 m to 3.2 m and decreasing connecting pipe diameter from 40 mm to 30 mm, maximum lost angle is shifted to the lower frequencies. By this way, maximum damping of the system occurs at lower frequencies where carbody is excited with strong vibrations.

PSD diagrams of first axle, front bogie frame and carbody vertical accelerations for two sets of air suspension parameters are shown in Fig. 22. As it can be seen from this figure, by adjusting air suspension parameters, transmitted low frequency vertical vibration to the carbody is reduced.

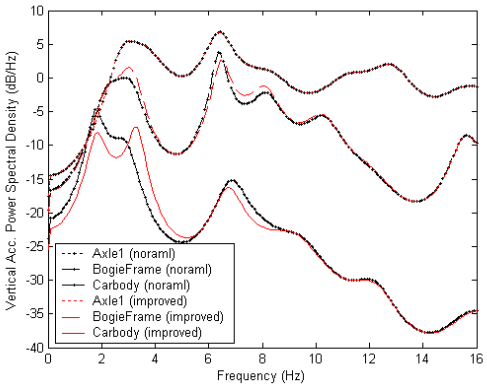

Fig. 22 PSD diagram of accelerations
$V_{normal} = 40\,Lit,\ L_{normal} = 2200\ mm, D_{normal} = 40\,mm$
$V_{improved} = 100\,Lit,\ L_{improved} = 3200\ mm, D_{improved} = 30\,mm$

For evaluation of achieved improvement in the system performances, Sperling ride comfort index introduced by Dukkipati [21], which is defined by following equation, is

implemented.

$$Wz = \left(\int_{0.5}^{30} a^3 B^3 df \right)^{1/10} \quad (12)$$

In the above equation, f is frequency, a is acceleration in frequency domain (cm/s^2) and B is defined by following equation:

$$A = (1 - 0.277 f^2)^2 + (1.563 f - 0.0368 f^3)^2$$
$$B = 0.588 \left[\frac{1.911 f^2 + (0.25 f^2)^2}{A} \right]^{1/2} \quad (13)$$

Fig. 23 shows the simulation results. As it can be seen, by simply modifying air suspension parameters, passengers' comfort and ride comfort index are improved.

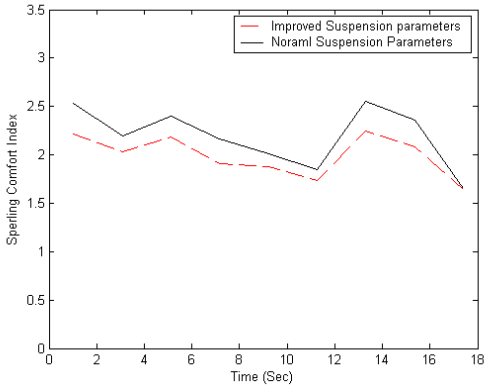

Fig. 23 Sperling ride comfort index for Tehran-Ghazvin route (Straight section) with 80 km/h speed

$V_{normal} = 40\,Lit,\ L_{normal} = 2200\ mm, D_{normal} = 40\,mm$
$V_{improved} = 100\,Lit,\ L_{improved} = 3200\ mm, D_{improved} = 30\,mm$

VII. Conclusion

This research work proposes a new nonlinear air spring model for studding air suspension components influences on the system behavior. This new model is validated by using real test data from field experiments and can be easily used in dynamic modeling of air springs. Comparison of the results shows good agreement between proposed model and test results that says this new model can be used for simulation of secondary suspension behaviors very well. Effects of air reservoir volume and connecting pipes' length and diameter on the system performances are investigated. By using achieved illustrative graphs about influences of air suspension parameters on the system behavior, and by estimating proper values for air suspension parameters, based on the design requirements in rail–vehicles, air suspension system isolates the vehicle from vibrations more and shows better performances. Results show that by using new set of suspension parameters, passengers' comfort is improved and ride comfort index is reduced about 10%.

Acknowledgment

Authors express their sincere thanks to Sharif University of Technology. They are grateful for the excessive support from Irankhodro Rail Transport Industries Co.

References

[1] Sun Y.Q., Dhanasekar M. (2002), "A dynamic model for the vertical interaction of the rail track and wagon system", International Journal of Solids and Structures; 39: 1337–1359.
[2] Hou K., Kalousek J., Dong R. (2003), "A dynamic model for an asymmetrical vehicle/track system", Journal of Sound and Vibration; 267: 591–604.
[3] Tanabe M., et al. (2003), "Computational model of a Shinkansen train running on the railway structure and the industrial applications", Journal of Materials Processing Technology; 140: 705–710.
[4] Durali M., Bahabadi M.M.J. (2004), "Investigation of train dynamics in passing through curves using a full model", Rail Conference, Proceedings of the ASME/IEEE Joint: 83 – 88.
[5] Li P., Goodall R., et al. (2007), "Estimation of railway vehicle suspension parameters for condition monitoring", Journal article, Control Engineering Practice; 15: 43–55.
[6] Zhang N., Xia H., et al (2008), "Vehicle–bridge interaction analysis under high-speed trains", Journal of Sound and Vibration; 309: 407–425.
[7] Banerjee N., et al (2008), "Bond graph modeling of a railway truck on curved track", Journal article, Simulation Modeling Practice and Theory, Available online.
[8] Boast D., Fellows S., Hale M. (2002), "Effects of temperature, frequency and amplitude on the dynamic properties of elastomers", conference paper, AVON Automotive; 03.
[9] Haupt P., Sedlan K. (2001), "Viscoplasticity of elastomeric materials: experimental facts and constitutive modeling", Journal article, Archive of Applied Mechanics; 71: 89-109.
[10] Berg M. (1998), "A non-linear rubber spring model for rail vehicle dynamics analysis", Journal of Vehicle system dynamics; 30: 197-212.
[11] Turner D. M. (1988), "A triboelastic model for the mechanical behaviour of rubber", Journal of Plastics and rubber processing and applications; 9: 197-201.
[12] Coveney V. A., Johnson D. E., Turner D. M. (1995), "A triboelastic model for the cyclic mechanical behaviour of filled vulcanizates", Journal of Rubber Chemistry and technology; 68: 660-670.
[13] Coveney V. A., Johnson D. E. (2000), "Rate-dependent modelling of a highly filled vucanizate", Journal of Rubber Chemistry and technology; 73(4): 565-577.
[14] Bergstrom J. S., Boyce M. C. (2000), "Large strain time-dependent behavior of filled elastomers", Journal of Mechanics of materials; 32: 627-644.
[15] Miehe C., Keck J. (2000), "Superimposed finite elastic-viscoelastic-plastoelastic stress response with damage in filled rubbery polymers Experiments, modelling and algorithmic implementation", Journal of Mechanics and physics of solids; 48: 323-365.
[16] Lion A. (1996), "A constitutive model for carbon black filled rubber: Experimental investigation and mathematical representation", Journal of Continuum Mechanics and Thermodynamics; 8: 153-169.
[17] Berg M. (1999), "A three-dimensional airspring model with friction and orifice damping", Journal of Vehicle System Dynamics; 33: 528–539.
[18] Presthus M. (2002), "Derivation of Air Spring Model Parameters for Train Simulation", Master dissertation, Department of applied physics and mechanical engineering, Division of fluid mechanics, LULEA University.
[19] Docquier N., Fisette P., Jeanmart H. (2007), "Multiphysic modelling of railway vehicles equipped with pneumatic suspensions", Journal of Vehicle System Dynamics; 45(6): 505–524.
[20] Sayyaadi H., Shokouhi N. (2009), "A New Model in Rail–Vehicles Dynamics Considering Nonlinear Suspension Components Behavior", Elsevier, International Journal of Mechanical Sciences; 51; 222–232.
[21] Dukkipati R. V., Harg V. K., (1984), "Dynamics of railway vehicle systems", Academic press, Harcourt Brace Jovanovich, Publishers.